Journal of
Applied and Computational Mechanics

Research Paper

Four Legged Guará Robot: From Inspiration to Implementation

Antônio Bento Filho[1], Cristiane Pescador Tonetto[2], Rafhael Milanezi de Andrade[3]

[1] Department of Mechanical Engineering, Universidade Federal do Espírito Santo, Vitória-ES, 29075-910, Brazil, Email: antonio.bento@ufes.br

[2] Department of Mechanical Engineering, Universidade Federal do Espírito Santo, Vitória-ES, 29075-910, Brazil, Email: cristiane.tonetto@ufes.br

[3] Department of Mechanical Engineering, Universidade Federal do Espírito Santo, Vitória-ES, 29075-910, Brazil, Email: rafhael.andrade@ufes.br

Abstract. Design of legged robots is still an open problem with several implementation challenges and there is little material available to guide new designs. Moreover, usually the actuator sets of the robot are heavy and bulky and are placed near the joints, which increases the weight and inertia of the legs and consequently results in instability, slower movement and high energy consumption. This paper presents the design, modeling, and control of the Guará, a sixteen-degree-of-freedom (DOF) legged robot, covering all stages of development of a quadruped robot, including experiments with a prototype. The system is composed by four legs, each one with 4 DOF. To reduce the leg's weight and inertia, here we present a design concept for the legs where the actuators are positioned on the robot platform and timing belt transmissions are used to drive the joints. Moreover, the design of the legs mimics the human leg by presenting the knees faced forward and its locomotion pattern mimics the quadruped wave gait. With this configuration, the robot is able to walk on straight lines or free curved paths. The control system of the robot consists of a high-level state machine and a lower level PID position controller. The electronics are embedded over a flat platform coupled to the legs. The kinematics of the robot was studied and an integrated environment was provided for walking simulation, adjustment, and diagnosis of operation. The experimental results are focused on the kinematics of the legs and the stability of the robot and show a good agreement between the designed and executed movements. This paper is presented as a framework that can be generalized to other systems and can be a useful reference for the design of other legged robots.

Keywords: Legged robot, Mobile robot, Quadruped, Biological inspiration, Kinematic, Wave gaits.

1. Introduction

Legged robots have been designed for different applications in the last few decades [1, 2, 3, 4, 5, 6, 7]. When compared to wheeled and tracked locomotion robots, legged robots present superior mobility in natural terrains, and they can be used for both flat and rough terrains [8]. On a smooth floor, legged robots can walk [9, 2], run [10, 3] and jump [8]. On rough ground or sloped terrains, they can change their postures to obtain appropriate stability [11, 12, 13]. These robots can also overcome obstacles during different types of activities, such as steps [14], rocks [15], among others.

The leg is a key point in the design of legged robots [16]. Depending on the task and type of terrain, legged robots need different mechanical leg characteristics. Kumar and Pathak [8] study a four legged jumping robot with compliant legs. The leg consists of two actuated joints: one in the hip, one in the knee of the robot; and a spring and damper in parallel in the shank. Chen et al. [9] present a six-legged robot, whose legs are composed by three actuator joints, two in the hip and one in the knee. The legs are similar to those of quadruped animals, but the knee of the first pair of legs is facing forward and the other two pairs are facing backward. Focchi et al. [17] present a four-legged robot for walking on a high-slope. The legs of the robot are similar to those presented in Chen et al. [9], with two actuated joints in the hip and one in the knee. Hoffmann and Simanek [18] presented a compliant legged with just one actuated joint in the robot hip and a passive rotation knee joint facing backward with springs attached. Rodriguez et al. [19] presented a mechanical scheme for a leg to be included in legged vehicles that simplifies the control actuations along the stride. Wu et al [20] designed a 16-legged robot as a carrying platform system. The robot is based on closed-chain reconfigurable legs to improve obstacle climbing and surmounting process. However, usually the actuators to drive the leg joints are heavy and bulky due to the high power required to move the robot [20, 21]. Furthermore, several designs consider the actuators integrated in the robot's leg, which increases the inertia and weight of the movable parts of the robot [8, 17, 22, 23]. For example, Kumar and Pathak [8] designed the robot's leg with a compliant actuator located on the distal part of the leg and Garcia et al. [24] considered the power train of the joints with cardan shaft and hypoid gears. Such design impairs the robot's leg agility and balance by increasing the dynamic effects of the leg [25]. To overcome these shortcomings, our solution considers the gear-motors, which represent most of the actuator's weight located in the robot platform and uses timing belts, which are lightweight, flexible and with low inertia, to synchronize the lower leg segments with the geared motors.
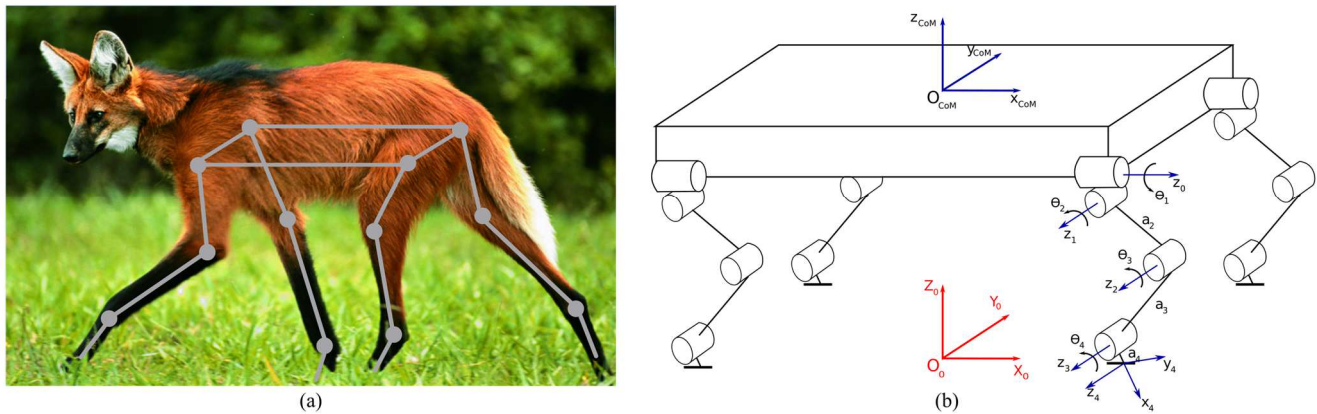
Fig. 1. Biologically inspired Guará robot. (a) Guará wolf with the inspired structure of the robot [35]. (b) robot schematic.

Contrasting the majority of leg designs cited above, the leg of the Guará robot uses four actuated joints [26, 27], with two DOFs in the hip, one in the knee, and one in the foot, to produce movements similar to those in quadruped animals. The joint actuators are positioned on the robot's platform to reduce the leg's weight and inertia. Moreover, the robot walks with the knees facing forward. This configuration lowers knee joint angles with small compensatory hip movements, avoiding reaching the kinematic limit of the knee joint. With four equal legs, the kinematics of the robot becomes simpler. This facilitates control and reduces the overall operating cost of the navigation system. In [27] it was presented an overview of the project to deal with obstacles overcoming concept. Here we bring up a complete methodology to build a quadruped robot from a mechanical point of view.

Robot navigation is another challenge to be designed. The navigational strategy adopted here was based on the walking of most quadruped animals in flat terrains [28] and it was implemented through a walking pattern for indoor navigation [26, 29]. In addition, the structure of the robot allows to implement several walking control strategies: meta stable locomotion [30], robot cooperation [31, 32], among others, which also makes the robot an interesting platform for research and teaching. There is an ongoing research in cooperating robot modelling for walking strategies with early results presented on [33].

This paper is organized as follows. The design of the legged robot Guará is presented in Section 2. Section 3 presents the forward and inverse kinematics, and the differential kinematics of the robot. Section 4 shows the walking pattern strategy, considering a straightforward and turning trajectory. The experimental results are shown in Section 5 and Section 6 presents the final remarks of this work.

2. Robot Design

In this section we present the robot design. The photo of a guará wolf is shown in Fig. 1 (a), it is a species of canid endemic to South America and a unique member of the genus Chrysocyon, and Fig. 1 (b) presents a schematic view of the robot, showing the world, *center of mass* (CoM), legs and feet reference frames (RF). The leg design resembles a four revolute joints manipulator, in which the RF origin is on the leg's joint. Each leg's RF origin has a position vector from CoM and the leg's joint RF are in accordance with Denavit-Hartenberg convention [34]. The general dimensions of the robot are given in Table 1.
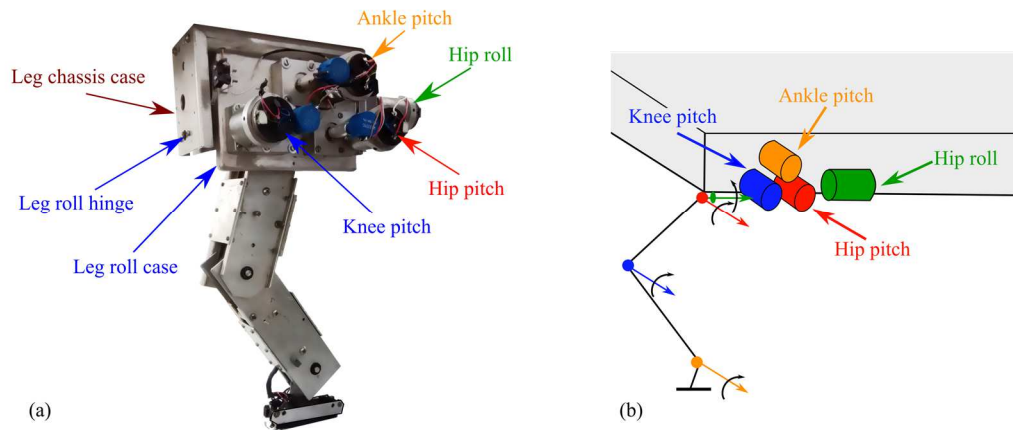
2.1 Leg design

The designed leg with four DOFs is shown in Fig. 2. Fig. 2 (a) show the built leg of the robot. The hip, knee, and ankle pitch DC gear-motors are placed in the leg roll case. The hip-roll joint DC gear-motor is placed on the leg chassis case. The design considers the gear-motors placed on the leg roll case to reduce the overall inertia of the leg to be driven by hip actuators. The hip pitch, knee, and ankle joints are driven by timing belts that connect the DC gear-motors to the joints. Fig. 2 (b) presents the schematic design of the leg's DOFs. Two DOFs provide the abduction-adduction (roll) and flexion-extension (pitch) of the hip joint; and two DOFs provide knee flexion-extension and ankle dorsiflexion-plantarflexion.

The locomotion of humans and animals is a complex phenomenon, with a great number of individual motions occurring simultaneously in the sagittal, frontal and horizontal planes. It is intuitive that, under these movements, the CoM translates in a path requiring the least energy consumption [36]. A normal step kinematics describes six movements [37, 38, 39, 36]. Hip and knee flexion/extension allow to increase and decrease the effective length of the leg to vary the stride length, flatten the inverted pendulum path of the hip, and smooth the transition between phases of leg support. Hip abduction/adduction allows for transferring the body's weight onto supporting legs during foot transition as shown in Fig. 3. For the robot to make turns, our first insight was to design the leg with a yaw DOF. However, looking at mammals, we see that their legs have higher hip-abduction/adduction (roll) than hip-rotation (yaw), so we decided to build the leg with a hip-roll DOF. The robot takes turns by varying the leg abduction/adduction in support-stroke and flight. Fig. 3 shows the lateral movement for legs abduction/adduction and the main dimensions in millimeters.

Table 1. Robot general dimensions

| Parameters	Value
Length between front and rear legs	0.390 m
Length between right and left legs	0.310 m
Thigh length	0.200 m
Shank length	0.200 m
Ankle length	0.050 m
Robot height	0.470 m
Robot weight	15.8 kgf

Fig. 2. Leg Design. (a) Overall leg as built. (b) Schematic of the leg. The leg is composed of four actuators, three for hip, knee, and ankle pitch and one for hip roll. The actuators are placed inside the leg chassis case.
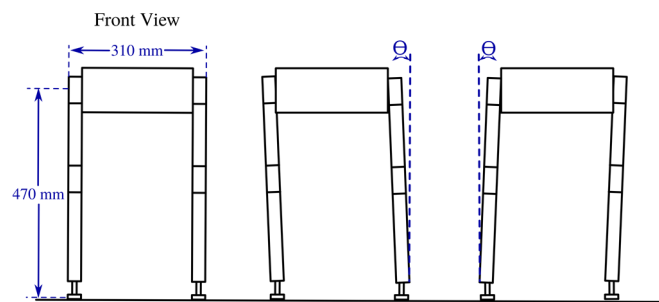
Fig. 3. Lateral movements enabled by the hip roll DOF to improve the robot's balance.
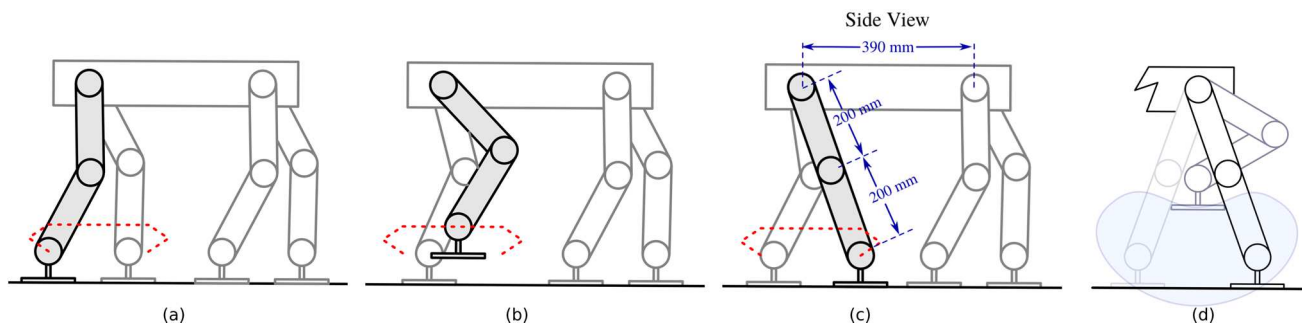
Fig. 4. Main movements and data of the leg: (a) Leg taking off, (b) Leg flighting, (c) Leg landing, (d) The leg workspace.

The mechanical approach for the leg uses a similar configuration and DOF layout as of a human leg. This is highly energy-efficient and, with the mechatronic design implemented for the legs, other shapes, like fore and hind limbs of a four-legged animal [40], would be easily implemented. As shown in Fig.2(b), the hip roll abduction/adduction gear-motor is mounted on the leg chassis case, which is fixed to the body of the robot. The hip roll and pitch axis intersect. Hip, knee, and ankle pitch flexion/extension gear-motors are mounted on the leg roll case, which rolls under hip roll gear-motor command. Finally, in this configuration, we used a flat foot, which allows for toe-off and heel-strike events to be implemented.

Figure 4 shows legs at work, the main dimensions of the legs and of the robot, and the movements of the legs. Figure 4 (a) shows the rear-right leg ready to take-off, then in Fig. 4 (b) it is flying and then in Fig. 4(c) it is landing to start new support-thrust cycle. The other legs are in the support-trust state, having their knees slightly bent. Figure 4 (d) shows the reachable workspace and kinematic limits for different configurations of hip and knee joints angles. The main dimensions of the side view are shown in Fig. 4(c).

Although the animals move with their fore and hind knees at inverted angles, the robot walks with both angled forward to simplify walking movements, to avoid legs collisions and to keep away from the joint's kinematic limits. We focus on making the robot develop straight and curved walking paths using the last leg link resembling a human foot.

2.2 Control architecture

Figure 5 shows the two levels control architecture of the robot, which was adopted to deal with on-the-fly math operations [25]. The matrix kinematics runs on a computer and the controllers of the angles of the legs run on onboard the robot. The two levels of control are wired together by a 1.2 megabits per second (Mbps) Control Area Network (CAN) bus [41].

Table 2. DH parameters for legs [34].

link	a_i	d_i	α_i	θ_i
1	0	0	$\pi/2$	θ_1
2	a_2	0	0	θ_2
3	a_3	0	0	θ_3
4	a_4	0	0	θ_4

The high-level system kernel is on a computer, which runs a walking kinematic model, stability criterion, communication, data acquisition, and display interface. The movement of the robot and its legs is shown on a graphic display, for off simulation purposes, and can be exported through a file saving application for debugging and foothold configuration analysis. The low level includes the controller boards for the legs onboard the robot. These boards run the communication and a PID joint angles controller. They have input-output (I/O) ports, the actuator gear-motors of the joints run through Pulse Width Modulation (PWM) outputs, and data acquisition is done from leg's angle transducer A/D converters.

3. Kinematics

The robot is composed by four legs, with four DOF each, connected by the platform. This configuration can be viewed as four robotic manipulators, coupled to a platform, and the operational space is defined by the points that can be reached by each foot. The kinematic model provides orientation for the body of the robot, with the data acquired from each leg joint potentiometer, and through it the trajectory coordinates of the foot are updated.

3.1 Forward Kinematics

The direct kinematics model computes the configuration of each link of the legs separately. Figure 6 depicts the main RF of the legs. We use Denavit-Hartenberg (DH) convention [26, 34], whose parameters for the leg are shown in Table 2.

Homogeneous transform from the legs to the CoM of the robot is obtained according to Eq. (1).

$$T_i^{CoM} = \begin{bmatrix} [R_i^{CoM}] & [d] \\ [0] & 1 \end{bmatrix} \tag{1}$$

where $[R_i^{CoM}]_{(3 \times 3)}$ is the rotation matrix between leg's and CoM's reference frames, $[d]_{(3 \times 1)}$ is the leg RF position vector referred to CoM and $[0] = [0\ 0\ 0]_{(1 \times 3)}$.
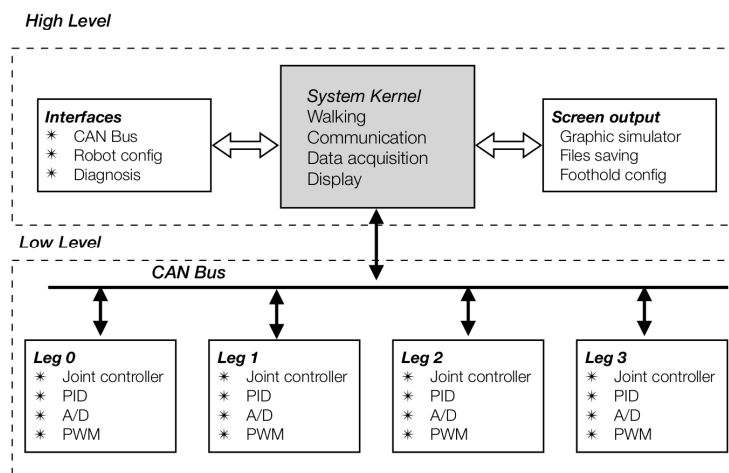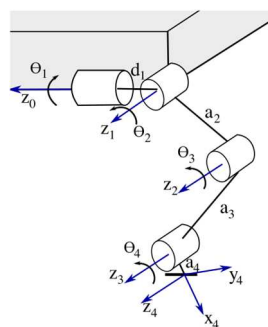

Fig. 5. Control architecture.

Fig. 6. Reference frames and variables for the legs.

Figure 6 shows DH parameters for one leg, which are replicated for the other legs. Each leg joint positions are achieved using homogeneous transformations, which are set up using DH convention parameters, in which $s_i=\sin(\theta_i)$ and $c_i=\cos(\theta_i)$ in matrix Eq. 2. It is worth mentioning that hip-roll and hip-pitch axis were designed to intersect. This way, the d_1 parameter (shown in Fig. 6) is null, since the axis origins are equal by construction.

$$A_i^{i-1} = \begin{bmatrix} c\theta_i & -s\theta_i c\alpha_i & s\theta_i s\alpha_i & a_i c\theta_i \\ s\theta_i & c\theta_i c\alpha_i & -c\theta_i s\alpha_i & a_i s\theta_i \\ 0 & s\alpha_i & c\alpha_i & d_i \\ 0 & 0 & 0 & 1 \end{bmatrix}$$

(2)

A set of homogeneous transform matrices, as shown in Eq. (3), is defined for each leg to map their joint and link variables in their RF.

$$A_1^0 = \begin{bmatrix} c_1 & 0 & s_1 & 0 \\ s_1 & 0 & -c_1 & 0 \\ 0 & 1 & 0 & 0 \\ 0 & 0 & 0 & 1 \end{bmatrix} A_2^1 = \begin{bmatrix} c_2 & -s_2 & 0 & a_2 c\theta_2 \\ s_2 & c_2 & 0 & a_2 s\theta_2 \\ 0 & 0 & 1 & 0 \\ 0 & 0 & 0 & 1 \end{bmatrix} A_3^2 = \begin{bmatrix} c_3 & -s_3 & 0 & a_3 c\theta_3 \\ s_3 & c_3 & 0 & a_3 s\theta_3 \\ 0 & 0 & 1 & 0 \\ 0 & 0 & 0 & 1 \end{bmatrix} A_4^3 = \begin{bmatrix} c_4 & -s_4 & 0 & a_4 c\theta_4 \\ s_4 & c_4 & 0 & a_4 s\theta_4 \\ 0 & 0 & 1 & 0 \\ 0 & 0 & 0 & 1 \end{bmatrix}$$

(3)

3.2 Inverse Kinematics

We used a geometric approach to solve the inverse position kinematics of the manipulator [34, 42]. It was applied for the four DOF leg the approach shown by Bonitz [43]. Regarding Fig. 6, we apply the cosine law between links 2 and 3 as follows:

$$D = \cos(\theta_3) = \frac{x_3^2 + y_3^2 + z_3^2 - (a_2^2 + a_3^2)}{2a_2 a_3}$$

$$\theta_3 = atan2 \left(\frac{\sqrt{1 - D^2}}{D} \right)$$

(4)

where x_3, y_3, and z_3 are the spatial coordinates of joint 3 RF origin O_3 and a_2 and a_3 are the lengths of links 2 and 3, respectively, as shown in Fig. 6, and we use *atan2* function to compute the arc-tangent taking into account the sign of both arguments to consider the angle quadrant.

$$\theta_1 = atan2 \left(\frac{x_3}{y_3} \right)$$

(5)

Similarly, for joint 0 and 2 we get:

$$\theta_2 = atan2 \left(\frac{z_3}{\sqrt{x_3^2 + z_3^2}} \right) - atan2 \left(\frac{a_3 sin\theta_3}{a_2 + a_3 cos\theta_3} \right)$$

(6)

In statically stable walking, link a_4 can be kept in a known fixed vertical θ_4 pitch angle, which allows the coordinates of joint 3 to be determined as follows:

$$\begin{bmatrix} ^0x_3 \\ ^0y_3 \\ ^0z_3 \end{bmatrix}^T = \begin{bmatrix} ^0x_4 - a_4 sin\theta_4 cos\theta_1 \\ ^0y_4 - a_4 sin\theta_4 sin\theta_1 \\ ^0z_4 - a_4 sin\theta_4 \end{bmatrix}$$

(7)

There are two roots for θ_3 in Eq. 4. The positive root was chosen, allowing knee-ahead (elbow-up) configuration for the leg. If a negative root is chosen, knee-behind (elbow-down) configuration, like fore limbs in a four-legged animal [40] is allowed. A singularity that occurs when $\theta_3=0$, is monitored while the robot is walking to avoid it.

3.3 Differential kinematics: Jacobian

The differential map relates the general velocity vector of the foot $[\dot{x}, \dot{y}, \dot{z}, \omega_x, \omega_y, \omega_z]^T$, with the joints velocity vector $[\dot{\theta}_1, \dot{\theta}_2, \dot{\theta}_3, \dot{\theta}_4]^T$, through the Jacobian **J**, by $[\dot{x}, \dot{y}, \dot{z}, \omega_x, \omega_y, \omega_z]^T = \mathbf{J(q)} [\dot{\theta}_1, \dot{\theta}_2, \dot{\theta}_3, \dot{\theta}_4]^T$, where $\mathbf{q} = [\theta_1 \ \theta_2 \ \theta_3 \ \theta_4]^T$ is the joint variables vector and the velocity components are expressed in leg RF. The differential map allows the speed analysis for the joints (e.g., maximum required speed) and trajectory planning by using differential kinematics. Equation (8) shows the Jacobian matrix [44] of the leg.

$$J(\boldsymbol{q}) = \begin{bmatrix} z_0 \times (p - p_0) & z_1 \times (p - p_1) & z_2 \times (p - p_2) & z_3 \times (p - p_3) \\ z_0 & z_1 & z_2 & z_3 \end{bmatrix}$$

(8)

where $z_{0...3}$ are joint axes, $p_{0...3}$ are joint position vectors and p is the foot position vector, all expressed in the leg RF. The (6×1) sub-matrices of the Jacobian matrix are given in Eq. (9).

$$J(\boldsymbol{\theta_1}) = \begin{bmatrix} -(a_2 c_2 + a_3 c_{23} + a_4 c_{234})s_1 \\ (a_2 c_2 + a_3 c_{23} + a_4 c_{234})c_1 \\ 0 \\ 0 \\ 0 \\ 1 \end{bmatrix} J(\boldsymbol{\theta_2}) = \begin{bmatrix} -(a_2 s_2 + a_3 c_{23} + a_4 s_{234})c_1 \\ (a_2 s_2 + a_3 c_{23} + a_4 s_{234})s_1 \\ (a_2 c_2 + a_3 c_{23} + a_4 s_{234})c_{21} \\ -s_1 \\ -c_1 \\ 0 \end{bmatrix} J(\boldsymbol{\theta_3}) = \begin{bmatrix} -(a_3 s_{23} + a_4 s_{234})c_1 \\ (a_3 s_{23} + a_4 s_{234})s_1 \\ (a_3 c_{23} + a_4 c_{234})c_{21} \\ -s_1 \\ -c_1 \\ 0 \end{bmatrix} J(\boldsymbol{\theta_4}) = \begin{bmatrix} -a_4 s_{234}c_1 \\ a_4 s_{234}s_1 \\ a_4 c_{234}c_{21} \\ -s_1 \\ -c_1 \\ 0 \end{bmatrix}$$

(9)

where $c_2=\cos(\theta_2)$, $c_{23}=\cos(\theta_2+\theta_3)$, $c_{234}=\cos(\theta_2+\theta_3+\theta_4)$, $s_1=\sin(\theta_1)$, $c_1=\cos(\theta_1)$, $s_{234}=\sin(\theta_2+\theta_3+\theta_4)$, and $c_{21}=\cos(\theta_2+\theta_1)$.

The Jacobian matrix of the leg $\mathbf{J(q)} = [J(\theta_1) J(\theta_2) J(\theta_3) J(\theta_4)]$ has *rank*=4, allowing to get the Moore-Penrose pseudo inverse $\mathbf{J}^+=(\mathbf{J}^T\mathbf{J})^{-1}\mathbf{J}^T$ [45] and the generalized contact force vector **F** on the foot from the generalized joint torque vector **T**, through the relationship $\mathbf{F}=\mathbf{J}^+\mathbf{T}$.
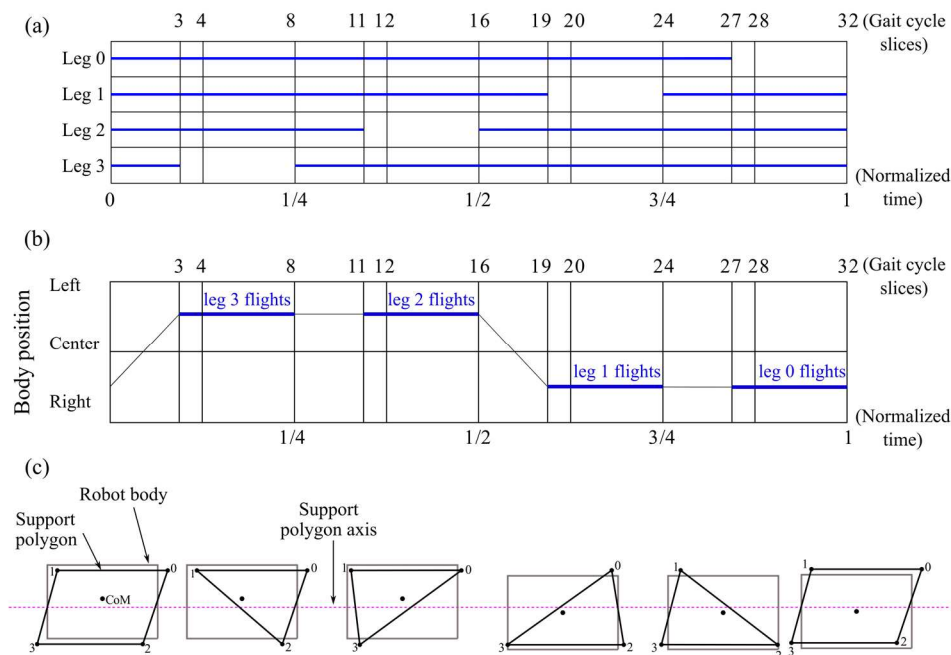
Fig. 7. Wave gait characteristics. (a) Regular symmetrical full cycle periodic wave gait. (b) Regular symmetrical full cycle periodic wave gait. (c) Full gait cycle support polygons.

4. Wave Gaits

These sections present the strategies and assumptions for gait planning and their implementation for the robot. Research on biomechanics of human beings, animals like quadrupeds and ground insects, has inspired the mathematical modeling of their locomotion. These models allow us to perform kinematic and dynamic simulations to understand their behavior and to infer about their physics. Scientific results allow for the construction of machines that could mimic behavior and abilities of animals [29, 46, 47, 48, 49, 50, 16].

4.1 Gait modeling

We use a regular symmetrical full cycle periodic natural sequence wave gait, as in [29], as shown in Fig. 7(a), to run the robot. The gait cycle is divided into 27 support-stroke slices and 5 flight slices, totaling 32 slices. Simultaneously, 4 legs are supported and pushed in 12 slices and 3 legs in 20 slices. For foot trajectory execution, the slice is divided in 2, 4, or 8 set-points, for better precision and to reduce foot slippage.

During push-forward, the body of the robot is laterally displaced, relative to the feet, to the opposite side of the next leg to fly. This synchronized movement is made to improve the stability in walking, as shown in Fig. 7(b). This allows for the CoM to be moved into the support polygon, as indicated in Fig. 7 (c), thereby increasing robot's statically stability margin (SSM) [30].

The gait parameters are the leg's loading factor $\beta=0.875$, which is the ratio between the normalized time of leg flighting and supporting, and the phase angles $\phi_0=0$, $\phi_1=0.75$, $\phi_2=0.5$ and $\phi_3=0.25$, which are the quotient between the time of the leg land and the total time [29]. The loading factor and the phase angles are taken from Fig. 7(a).

4.2 Turning gait

Figure 8 shows the relative positions of the body of the robot and its legs in stroke while turning. The robot performs incremental small arcs θ with CoM radius R_{CoM}, and external R_e and internal R_i curvature radius. Each θ increment defines λ_i and λ_e, respectively, internal and external strokes of the incremental turning step width. To perform a R_{CoM} right turn, as shown in Fig. 8, the inner and outer leg's stroke becomes $\lambda_i=R_i\theta\cos(\theta)$ and $\lambda_e=R_e\theta\cos(\theta)$. The four-legged turning, besides being an on-the-fly position vector rotation problem, was geometrically modeled in a very simple way by adding λ_e and λ_i to the straight walk increments of the feet. It becomes even simpler from the hardware point-of-view because these angular increments are added to the foot coordinates in the operating space of the legs, before being mapped to their joint space.

There is some complacency in the links, belts, and connection of the legs to the platform. Such compliance allows for absorption of small discontinuities that arise during the not synchronized incremental pushing of the legs while turning. These discontinuities also impair small variations in R_{CoM} radius, also absorbed by the overall compliance of the leg system.

5. Results and Discussion

After design and modeling, a prototype of the robot was built, as shown in Fig. 9. The legs are connected to an aluminum platform, on which are assembled the controller, power and communication hardware boards.

For the purposes of kinematic analysis, the platform and legs are supposed to be a system of rigid bodies. The leg footholds form a plane parallel to the bearing surface if neither foothold is on an elevation or depression on the floor.

The foot's path is shown in Fig. 10. Dot lines are references sent and continuous lines are the executed path by onboard robot controller. The ideal path for flight of the foot to a new stroke position would be a cycloid. However, due to small disturbances, the foot starts taking-off while it is still in support or it is still moving ahead flying to a new stroke position and then lands. In both situations, the foot forward motion pushes back the robot, worsening its balance. We use a polygonal path, as shown by the red dot lines in Fig. 4 (a), (b) and (c), with foot take-off and landing velocities synchronized with the robot's velocity, which improves the overall balance, even though some small deviations still occur when the foot lands.
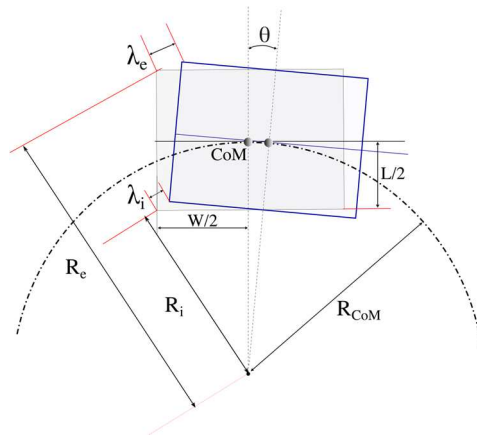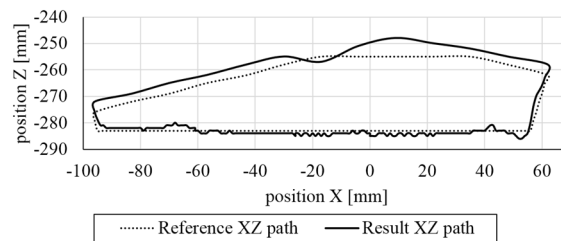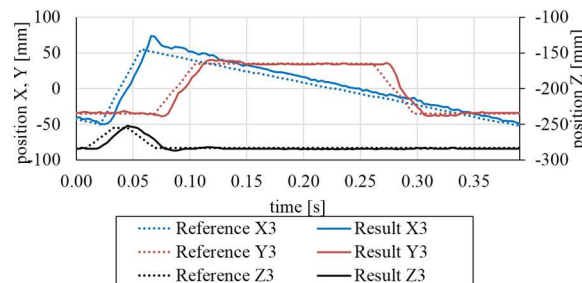
Fig. 8. Turning kinematics. θ is the curve angle increment. λ_i and λ_e are the internal and external stroke incremental step width, respectively. R_e and R_i are the external and internal curvature radius, respectively. R_{CoM} are the CoM curvature radius.


Fig. 9. The Guará Robot as built.

**Fig. 10.** Full step foot XZ coordinates.

Fig. 11. X, Y and Z coordinates for full step of foot 3.

Figure 11 shows foot references sent to and received from the robot. Dot lines are reference sent and continuous lines are executed by onboard robot controllers. They represent a complete gait cycle in the foot's operational space. The blue curves are the foot X coordinates. The first steep curve segment is the foot flying to a new stroke position. The second segment is the foot support-thrust cycle between the leg's fore and hind kinematic limits. The red curves are the foot Y coordinates which push the body side movement. The black curves are the foot Z coordinates, which the straight line part represents support-stroke phase and the curved line part describes the foot take-off, flight and landing. The first step segment of the blue line, up to the curve peak, is the foot going forward to a new stroke position and the second segment is the foot supporting and thrusting the robot.
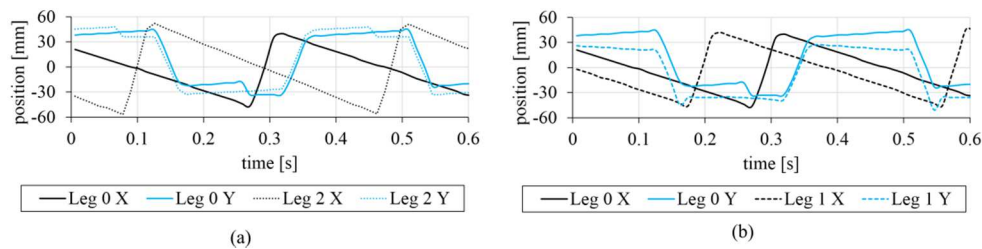
Fig. 12. Feet curved paths: (a) Feet 0 and 2, X-Y coordinates, (b) Feet 0 and 1, X-Y coordinates.
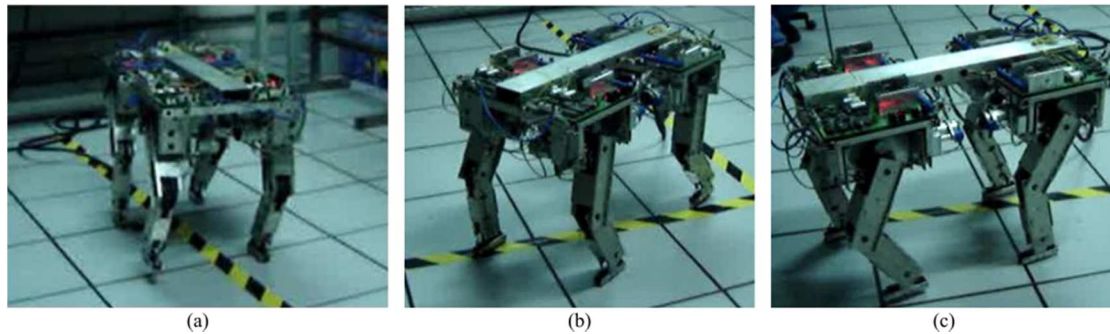
Fig. 13. Robot's turning right with average radius 1400 mm: (a) Start turning, (b) Middle path turning, (c) Ending turn.

The individual paths planned for the feet are generated in the high-level controller, according to the walking scheme previously discussed, and are tracked by the low-level onboard controllers. In Fig. 12 are shown these paths with the robot turning right with a 1.4 m radius. They are sampled using 4 set-points per slice, totaling 128 set-points for trajectory planning, each with up to 2.4 ms, with 108 thrusting and 20 flying points.

Figure 12 (a) shows front feet 0 and 2 foothold paths, referred to their leg joint 0 reference frame. Continuous and dot blue lines correspond to the lateral Y path, pushing the robot's body CoM towards inside support polygon. According to the turning model proposed, the front-left and front-right feet 0 and 2, perform paths λ_e and λ_i, pointing towards the curvature center. Symmetrically, rear-left and rear-right feet 1 and 3 perform paths pointing ahead of the curvature center. Continuous and dot black lines in Fig. 12 (a) correspond to foot 0 and 2 thrust X coordinate path. It can be seen that the dot black curve has greater amplitude (from bottom to upper corner) than the continuous one because foot 0 is turning outside the curve and has to travel a greater distance than foot 2 turning inside.

Figure 12 (b) depicts the same scenario as in Fig. 12 (a) but for left feet 0 and 1. Their path increments λ_e have same length but the foot 0 path points towards the curvature center and the foot 0 path points ahead of it. Such behavior agrees with Fig. 8. Here, the continuous and dashed black lines correspond to feet 0 and 1 thrust X path, which have the same amplitude, from the bottom to upper corners, as they have the same curvature radius and consequently travel equal distances. The discontinuities shown in lateral Y path, in Fig. 12, push the robot's body CoM towards inside support polygon and are due to the additional leg excursion necessary to lift the foot vertically. In this movement, the kinematics require not only the leg's extension or retraction but also an increase or decrease in the leg's joint 0 angle, which allow the leg to fly to a new stroke position. In summary, the feet in support move the robot's body according to the modeled foot movements, which are reflected in the robot's body, allowing it to walk straight and curved paths pushed by its legs.

Frames taken from robot's video doing a ninety degree right turn are shown in Fig. 13. In Fig. 13 (a), it can be seen the right front and hind legs have joint 0 (roll) symmetrical angles. The same can be seen for left legs, in mid-turn as seen in Fig. 13 (b), and in ending turn as seen in Fig. 13 (c), which validates the software approach to implement the turning robot on-the-flight.

6. Conclusions and Future Work

We presented the design, construction, and testing of the Guará, a four-legged sixteen DOF mobile robot. Special attention was given to the design of the leg as an alternative solution for previously legged robot projects. The use of a drive system based on timing belts enabled a lightweight and low inertia layout for the leg. The concentration of gear-motors as unsprung mass in the robot platform proved to be an important solution to improve the control and balance of the robot. The design of the legs, with a hip-abduction/adduction (roll) DOF rather than a hip-yaw DOF, allowed us to implement an important movement observed in mammals to displace laterally the body CoM towards the support polygon. From the walking control point of view, line segments were used in the feet workspace to generate straight and curved paths, and to synchronize the robot's body lateral movement. They were generated separately in the operating space and the final path as their vector sum, whose result was mapped to joint space by inverse kinematics. With this methodology, the robot was capable of walking straight lines and free curved paths, making turns on the flight and synchronizing walking and balance movements.

The results achieved here encourage future work and we think there are some important points that are worth mentioning. The successful humanoid's stability strategies, such as zero moment point (ZMP), instantaneous capture points (ICP), and centroidal moment pivot (CMP) [30, 51, 52], can be applied to study their role in the robot's kinematic. The actual high-level control program can be improved to perform heel-strike and toe-off, which are gait events that are not yet performed and present only sophisticated humanoid robots performing straight-leg walking [53]. We also recommend configuring the fourth link of the leg like metatarsal and metacarpal bones as in guará wolf, lions, dogs, and others speedy animals, to study their role in robot's kinetics.

Author Contributions

A.B. Filho developed the robot modeling, mechanics and software, initiated the project, and performed the experiments; C.P. Tonetto conducted further experiments, developed the graphics output and overall paper design; R.M. de Andrade developed the mathematical modeling, examined the theory validation and future work. The manuscript was written through the contribution of all authors. All authors discussed the results, reviewed, and approved the final version of the manuscript.

Conflict of Interest

The authors declared no potential conflicts of interest with respect to the research, authorship, and publication of this article.

References

[1] Bares, J. E., Wettergreen, D. S., Dante II: Technical description, results, and lessons learned, *International Journal of Robotics Research*, 18, 1999, 621-649.
[2] Kar, D. C., Design of Statically Stable Walking Robot: A Review, *Journal of Robotic Systems*, 20, 2003, 671-686.
[3] Raibert, M., Blankespoor, K., Nelson G., Playter, R., BigDog, the Rough-Terrain Quadruped Robot, *IFAC Proceedings Volumes*, 41, 2008, 10822-10825.
[4] Ponticelli, R., Garcia, E., Gonzalez de Santos P., Armada, M., A scanning robotic system for humanitarian de-mining activities, *Industrial Robot: An International Journal*, 35, 2008, 133-142.
[5] Gonçalves, R. S., Carvalho, J. C. M., A mobile robot to be applied in high-voltage power lines, *Journal of the Brazilian Society of Mechanical Sciences and Engineering*, 37, 2015, 349-359.
[6] Dharmawan, A. G., Hariri, H. H., Soh, G. S., Foong, S., Wood, K. L., Design, Analysis, and Characterization of a Two-Legged Miniature Robot With Piezoelectric-Driven Four-Bar Linkage, *Journal of Mechanisms and Robotics*, 10(2), 2018, 021003.
[7] Lin, R., Guo, W. , Li, M., Novel Design of Legged Mobile Landers With Decoupled Landing and Walking Functions Containing a Rhombus Joint, *Journal of Mechanisms and Robotics*, 10(6), 2018, 061017.
[8] Kumar, G., Pathak, P. M., Dynamic modelling & simulation of a four legged jumping robot with compliant legs, *Robotics and Autonomous Systems*, 61, 2013, 221-228.
[9] Chen, G., Jin, B., Chen, Y., Inverse Kinematics Solution for Position--Orientation Adjustment Algorithm of Six-Legged Robot Based on Geometry Structure, *Iranian Journal of Science and Technology, Transactions of Mechanical Engineering*, 40, 2016, 131-137.
[10] Heim, S. W., Ajallooeian, M., Eckert, P., Vespignani, M., Ijspeert, A. J., On designing an active tail for legged robots: simplifying control via decoupling of control objectives, *Industrial Robot: An International Journal*, 43, 2016, 338-346.
[11] Rebula, J. R., Neuhaus, P. D., Bonnlander, B. V., Johnson, M. J., Pratt, J. E., A Controller for the LittleDog Quadruped Walking on Rough Terrain, *Proceedings 2007 IEEE International Conference on Robotics and Automation*, Roma, 2007, 1467-1473.
[12] Chen, G., Jin, B., Chen, Y., Nonsingular fast terminal sliding mode posture control for six-legged walking robots with redundant actuation, *Mechatronics*, 50, 2018, 1-15.
[13] Kanner, O. Y., Dollar, A. M., Kinematic Design of an Underactuated Robot Leg for Passive Terrain Adaptability and Stability, *Journal of Mechanisms and Robotics*, 5(3), 2013, 031006.
[14] Nowicki, M. R., Belter, D., Kostusiak, A., CÏûek, P., Faigl J., Skrzypczynski, P., An experimental study on feature-based SLAM for multi-legged robots with RGB-D sensors, *Industrial Robot: An International Journal*, 44, 2017, 428-441.
[15] Kimura, H., Fukuoka, Y., Cohen, A. H., Adaptive Dynamic Walking of a Quadruped Robot on Natural Ground Based on Biological Concepts, *The International Journal of Robotics Research*, 26, 2007, 475-490.
[16] Garcia, E., Arevalo, J. C., Cestari, M., Sanz-Merodio, D., On the Technological Instantiation of a Biomimetic Leg Concept for Agile Quadrupedal Locomotion, *Journal of Mechanisms and Robotics*, 7(3), 2015, 301005.
[17] Focchi, M., del Prete, A., Havoutis, I., Featherstone, R., Caldwell, D. G., Semini, C., High-slope terrain locomotion for torque-controlled quadruped robots, *Autonomous Robots*, 41, 2017, 259-272.
[18] Hoffmann, M., Simanek, J., The Merits of Passive Compliant Joints in Legged Locomotion: Fast Learning, Superior Energy Efficiency and Versatile Sensing in a Quadruped Robot, *Journal of Bionic Engineering*, 14, 2017, 1-14.
[19] Rodriguez, A. G., Rodriguez, A. G., Rea, P. , A new articulated leg for mobile robots, *Industrial Robot: An International Journal*, 38, 2011, 521-532.
[20] Wu, J., Yao, Y.-a, Li, Y., Wang, S., Ruan, Q., Design and Analysis of a Sixteen-Legged Vehicle With Reconfigurable Close-Chain Leg Mechanisms, *Journal of Mechanisms and Robotics*, 11(5), 2019, 055001.
[21] Andrade, R. M., Bonato, P., The Role Played by Mass, Friction and Inertia on the Driving Torques of Lower-Limb Gait Training Exoskeletons, *IEEE Transactions on Medical Robotics and Bionics*, 2021, DOI: 10.1109/TMRB.2021.3052014.
[22] Andrade, R. M., Filho, A. B., Vimieiro, C. B. S., Pinotti, M., Evaluating Energy Consumption of an Active Magnetorheological Knee Prosthesis, *19th IEEE International Conference on Advanced Robotics (ICAR)*, Belo Horizonte, 2019, 75-80.
[23] Andrade, R. M., Martins, J. S. R., Pinotti, M., Filho, A. B., Vimieiro, C. B. S., Novel active magnetorheological knee prosthesis presents low energy consumption during ground walking, *Journal of Intelligent Material Systems and Structures*, 2021, DOI: 10.1177/1045389X20983923.
[24] Garcia, E., Galvez, J. A., de Santos, P. G., A mathematical model for real-time control of the SILO4 leg, *Proc. Int. Conf. Climbing and Walking Robots*, 2000.
[25] Andrade, R. M., Sapienza, S., Bonato, P., Development of a "transparent operation mode" for a lower-limb exoskeleton designed for children with cerebral palsy, *2019 IEEE 16th International Conference on Rehabilitation Robotics (ICORR)*, Toronto, 2019, 512-517.
[26] Bento Filho, A., Modeling, Gait Control and Obstacle Surpassing of the Guará, a Four Legged Robot with Four DOF in Each Leg, Brazil, Federal University of Espírito Santo, 2007.
[27] Bento A., Amaral, F, P. F. S., Pinto, B. G. M., A four legged walking robot with obstacle overcoming capabilities, *3rd Conference on Human System Interactions (HSI)*, 2010.
[28] McGhee, R. B., Frank, A. A., On the stability properties of quadruped creeping gaits, *Mathematical Biosciences*, 3, 1968, 331-351.
[29] Song, S. M., Waldron, K. J., Machines that walk: the adaptive suspension vehicle, *The MIT Press*, 1989, 315.
[30] Byl, K., Metastable Legged-Robot Locomotion, *Massachusetts Institute of Technology*, 2008.
[31] Ribeiro, L., Martins, D., Screw-Based relative Jacobian for manipulators cooperating in a task using Assur virtual chains, *20th International Congress of Mechanical Engineering*, 2010, 729-738.
[32] Tonetto, C. P., Rocha, C. R., Simas, H., Dias, A., Kinematics Programming for Cooperating Robotic Systems, *Technological Innovation for Value Creation*, Berlin, 2012.
[33] Tonetto, C. P., Bento A. F., Dias, A., Modeling of a Four-Legged Robot with Variable Center of Mass as a Cooperative Multirobot System, *International Symposiu on Multibody Systems and Mechatronics (MuSMe-2017): Multibody Mechatronic Systems*, 2018.
[34] Spong, M. W., Hutchinson, S., Vidyasagar, M., *Robot modeling and control*, Wiley New Jersey, 2006.
[35] Carvalho, C. T., Vasconcellos, E. M., Disease. Food and reproduction of the maned wolf - chrysocyon brachyurus (Illiger) (carnivora, canidae) in southeast brazil, *Revista Brasileira de Zoologia*, 21(3), 1995, 627-640.
[36] Rose, J., Gamble, J. G., *Human walking*, 2nd ed., Lippincott Williams and Wilkins, 1994.

[37] Inman, V. T., Eberhart, H. D., The major determinants in normal and pathological gait, *The Journal of Bone and Joint Surgery*, 35-A(3), 1953, 543-558.

[38] McMahon, T. A., *Muscles, reflexes, and locomotion*, New, Jersey: Princeton University Press, 1984.

[39] McMahon, T. A., Mechanics of locomotion, *The International Journal of Robotics Research*, 3(2), 4-28, 1984.

[40] Griffin, T. M., Main, R. P., Farley, C. T., Biomechanics of quadrupedal walking: how do four-legged animals achieve inverted pendulum-like movements?, *The Journal of Experimental Biology*, 207(20), 2004, 3545-3558.

[41] Di Natale, M., Zeng, H., Giusto, P., Ghosal, A., *Understanding and using the controller area network communication protocol: theory and practice*, Springer Science & Business Media, 2012.

[42] Mukanova, B. Control of Actuators Torques for Optimal Movement along a Given Trajectory for the DexTAR Robot, *Journal of Applied and Computational Mechanics*, 7(1), 2021, 165-176.

[43] Bonitz, R. G., Mars surveyor98 lander MVACS robotic arm control system design concepts, *Proceedings of the 1997 {IEEE} International Conference on Robotics and Automation*, 1997.

[44] Sciavicco, L., Siciliano, B., Sciavicco, B., *Modelling and Control of Robot Manipulators*, Heidelberg: Springer-Verlag, Berlin, 2000.

[45] Petkov, P. H., Christov, N. D., Konstantinov, M. M., *Computational methods for linear control systems*, Prentice Hall International (UK) Ltd., 1991.

[46] Schmiedeler, J. P., Waldron, K. J., The mechanics of quadrupedal galloping and the future of legged vehicles, *The International Journal of Robotics Research*, 18, 1999, 1224-1234.

[47] Migliore, S. A., Brown, E. A., DeWeerth, S. P., Biologically inspired joint stiffness control, *Proceedings of the 2005 {IEEE} International Conference on Robotics and Automation*, 2005.

[48] Semini, C., Tsagarakis, N. G., Guglielmino, E., Focchi, M., Cannella, F., Caldwell, D. G., Design of HyQ–a hydraulically and electrically actuated quadruped robot, *Proceedings of the Institution of Mechanical Engineers, Part I: Journal of Systems and Control Engineering*, 225(6), 2011, 831-849.

[49] Tournois, G., Focchi, M., Prete, A. D., Orsolino, R., Caldwell, D. G., Semini, C., Online payload identification for quadruped robots, *2017 {IEEE/RSJ} International Conference on Intelligent Robots and Systems, {IROS} 2017*, Vancouver, Canada, 2017, 24-28.

[50] Mikić, D., Desnica, E., Radivojević, N., Ašonja, A. Milićević, V., Software modeling of multi-degree-of-freedom motion system using matrices, *Journal of the Brazilian Society of Mechanical Sciences and Engineering*, 39, 2017, 3621-3633.

[51] Popovic, M. B., Goswami, A. Herr, H., Ground reference points in legged locomotion: Definitions, biological trajectories and control implications, *The International Journal of Robotics Research*, 24, 2005, 1013-1032.

[52] Popovic, M., Hofmann, A., Herr, H., Angular momentum regulation during human walking: biomechanics and control, Robotics and Automation, *IEEE International Conference on Robotics and Automation, 2004. Proceedings. ICRA '04. 2004*, New Orleans, LA, USA, 2004, 2405-2411.

[53] Griffin, R., Cobb, T., Craig, T., Daniel, M., van Dijk, N., Gines, J., Kramer, K., Shah, S., Siebinga, O., Smith, J., Neuhaus, P., Stepping Forward with Exoskeletons: Team IHMCś Design and Approach in the 2016 Cybathlon, *IEEE Robotics Automation Magazine*, 24, 2007, 66-74.

[54] Garcia, E., Galvez, J. A., de Santos, P. G., A mathematical model for real-time control of the SILO4 leg, *Proc. Int. Conf. Climbing and Walking Robots*, Madrid, Spain, 2000.

ORCID iD

Antônio Bento Filho https://orcid.org/0000-0002-2705-9294
Cristiane Pescador Tonetto https://orcid.org/0000-0002-0857-5023
Rafhael Milanezi de Andrade https://orcid.org/0000-0002-2839-3649

Publisher's Note Shahid Chamran University of Ahvaz remains neutral with regard to jurisdictional claims in published maps and institutional affiliations.